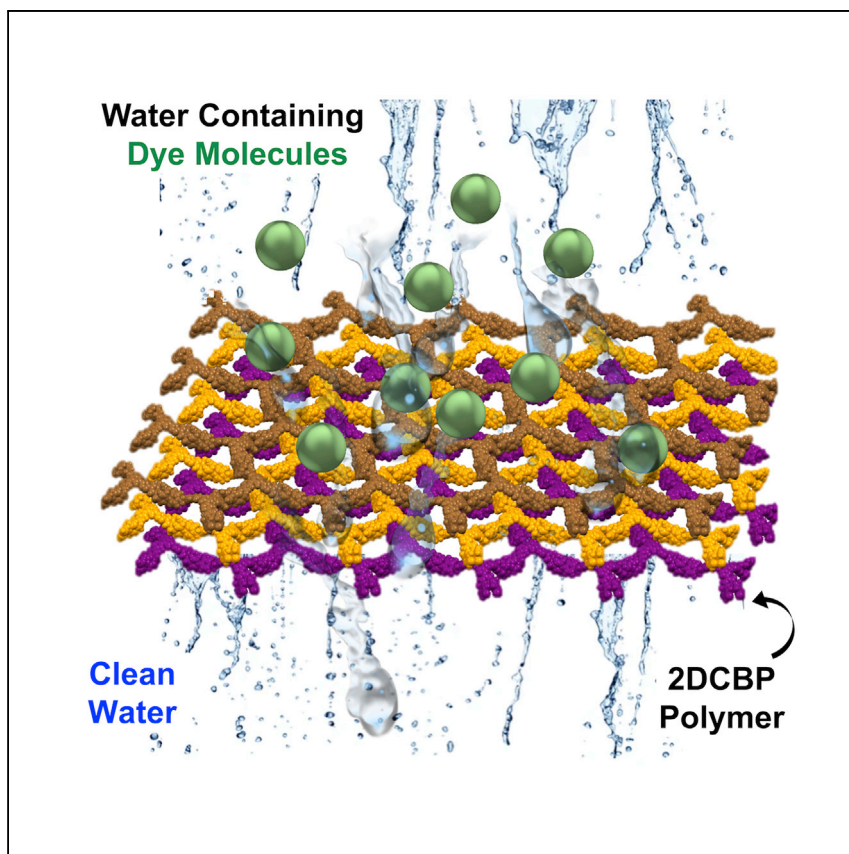


Article

# Cyclophane-based two-dimensional polymer formed by an interfacial click reaction



Copper-catalyzed azide-alkyne cycloaddition (CuAAC) reactions are efficient and selective, but challenges remain in using it to prepare crystalline two-dimensional (2D) polymers. Here, Roy et al. show that a cyclophane-based, highly crystalline, 2D polymer synthesized by CuAAC at a liquid-liquid interface can become useful in making state-of-the-art nanofiltration membranes for water purification.

Indranil Roy, Austin M. Evans, Partha Jyoti Das, ..., Joseph T. Hupp, William R. Dichtel, J. Fraser Stoddart

stoddart@northwestern.edu

### Highlights

Cyclophane-based building blocks have been used for 2D polymer synthesis

Interfacial polymerization utilizing CuAAC reaction produces crystalline 2D polymer

The polymer possesses multilayered faceted sheets-like morphology

The polymer has been used for nanofiltration membrane applications

Article

# Cyclophane-based two-dimensional polymer formed by an interfacial click reaction

Indranil Roy,<sup>1</sup> Austin M. Evans,<sup>1</sup> Partha Jyoti Das,<sup>1</sup> Mohamed Ateia,<sup>1</sup> Matthew R. Ryder,<sup>2</sup> Leighton O. Jones,<sup>1</sup> Masoud Kazem-Rostami,<sup>1</sup> Subhadip Goswami,<sup>1</sup> Yassine Beldjoudi,<sup>1</sup> Dengke Shen,<sup>3</sup> George C. Schatz,<sup>1</sup> Joseph T. Hupp,<sup>1</sup> William R. Dichtel,<sup>1</sup> and J. Fraser Stoddart<sup>1,4,5,6,7,\*</sup>

## SUMMARY

Two-dimensional polymers (2DPs) that incorporate molecular hosts offer a distinctive combination of properties, including covalent connectivity, structural regularity, chemical stability, permanent porosity, and molecular recognition. These features make these topologically planar macromolecular sheets promising in relation to applications, including those that appear in sensors, organic electronics, and nanofiltration membranes. Here, we use copper-catalyzed azide-alkyne click chemistry to construct a cyclophane-based 2DP at a liquid-liquid interface by polymerizing a bisazide-functionalized tetracationic cyclophane monomer with a 1,3,5-triethynylbenzene node. The 2DP prepared by employing this strategy is observed to be crystalline porous sheets by a combination of synchrotron X-ray diffraction, transmission electron microscopy, electron diffraction, and nitrogen porosimetry. When employed as the active layer in nanofiltration membranes, this 2DP exhibits excellent rejection performance of a dye, Brilliant Blue G, with 99% of the dye being removed after each cycle. Our findings could lead to the broad application of interfacial click polymerizations to produce 2DPs.

## INTRODUCTION

Cyclophanes are hollow host molecules that have been identified,<sup>1,2</sup> in some cases, for their extraordinary molecular recognition properties through noncovalent bonding interactions, usually involving their aromatic fence-like peripheries. Since their initial synthesis,<sup>3</sup> the modularity of cyclophanes' chemical functionality, cavity size, photophysical properties, and rich host-guest chemistry<sup>4</sup> has resulted in their capturing the attention<sup>5</sup> of chemists, materials scientists, and biologists. Over the years, they have been used not only in molecular recognition<sup>2</sup> but also in the production of mechanically interlocked molecules<sup>6</sup> and artificial molecular machines,<sup>7</sup> not to mention applications, such as polyaromatic hydrocarbon extraction,<sup>8</sup> sensing,<sup>9</sup> electron transfer,<sup>10</sup> catalysis,<sup>11</sup> molecular electronics,<sup>12</sup> live-cell imaging,<sup>13</sup> and drug delivery.<sup>14</sup> The majority of these applications, however, are limited to the solution phase, leaving limitless possibilities for these hosts to be employed as building blocks in the solid state. In a general context, the deployment of cyclophanes as structural building blocks for robust nanostructured materials<sup>15</sup> is an appealing goal.

Cyclophanes are straightforward to functionalize<sup>2</sup> and can therefore be developed as monomers suitable for use in polymerizations. If covalent bond-forming reactions, used to connect cyclophane subunits,<sup>15</sup> are confined (Figures 1A and 1B) to the

<sup>1</sup>Department of Chemistry, Northwestern University, 2145 Sheridan Road, Evanston, IL 60208, USA

<sup>2</sup>Neutron Scattering Division, Oak Ridge National Laboratory, Oak Ridge, TN 37831, USA

<sup>3</sup>Institutes of Physical Science and Information Technology, Anhui University, Hefei 230601, China

<sup>4</sup>School of Chemistry, University of New South Wales, Sydney, NSW 2052, Australia

<sup>5</sup>Institute of Molecular Science, Department of Chemistry, Zhejiang University, Hangzhou 310027, China

<sup>6</sup>ZJU-Hangzhou Global Scientific and Technological Innovation Center, Hangzhou 311215, China

<sup>7</sup>Lead contact

\*Correspondence: [stoddart@northwestern.edu](mailto:stoddart@northwestern.edu)  
<https://doi.org/10.1016/j.xcrp.2022.100806>

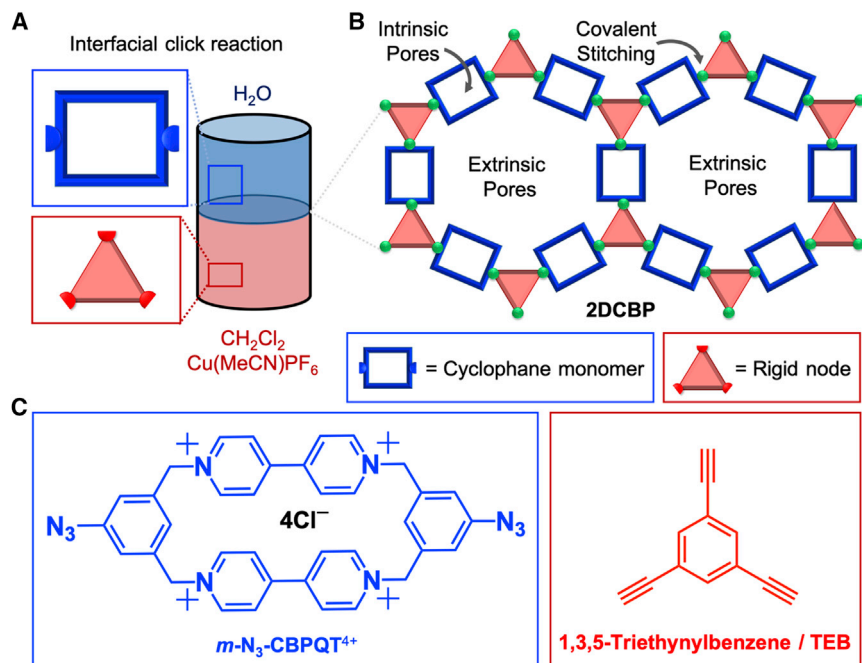


**Figure 1. Schematic representation of the interfacial click polymerization strategy used in the synthesis of 2DCBP**

(A) Click polymerization at the liquid-liquid interface between a monomer (blue cartoon) and a node (coral red cartoon).

(B) Interfacial 2D polymerization of a semi-rigid, box-like, tetracationic cyclophane monomer with two peripheral polymerizable groups and a rigid node with a minimum of three polymerizable groups yields 2DCBP with intrinsic and extrinsic pores.

(C) Structural formulas of the monomer and the node used in the construction of 2DCBP. The monomer ( $m\text{-N}_3\text{-CBPQT}^{4+}$ ) results from connecting two  $\text{BIPY}^{2+}$  units in an end-to-end fashion with two azide-functionalized  $m$ -xylylene linkers. The node, 1,3,5-triethynylbenzene (TEB), is available commercially.

molecular planes of the cyclophanes, macromolecular sheets with well-defined intrinsic pores<sup>16</sup> based on the cyclophane cavities, and extrinsic pores formed by structurally regular polymerization, can be produced. These two-dimensional polymers (2DPs) offer a distinctive combination of properties, including covalent connectivity, chemical stability,<sup>17</sup> structural regularity,<sup>18</sup> and permanent porosity.<sup>19</sup> All these properties arise from the two-dimensional (2D) network, together with the anticipated dual-pore morphology and molecular recognition capabilities that originate from the cyclophane monomers. As such, cyclophane-based 2DPs constitute a new class of topologically planar macromolecular sheets that hold promise for a wide range of technologically relevant applications, including their incorporation in chemical sensors,<sup>20–23</sup> nanofiltration membranes,<sup>24–27</sup> and organic electronics.<sup>28–30</sup>

We have prepared (Figure 1A) a cyclophane-based 2DP—hereafter referred to as 2DCBP—utilizing azide-alkyne polymerization at a liquid-liquid interface. To date, the majority of successful 2D polymerizations rely<sup>31–33</sup> on dynamic bond-forming reactions, such as boron-based<sup>34</sup> or Schiff-based<sup>35</sup> condensations, which are assumed to be able to anneal structural defects during polymerization. Recent research,<sup>36–42</sup> however, has shown that irreversible bond-forming reactions can also be utilized in 2D polymerizations when monomer species are preorganized by structure-directed syntheses at an interface. These recent reports prompted us to explore the high fidelity associated with azide-alkyne chemistry<sup>43,44</sup> at interfaces for carrying out 2D polymerizations. It is worth

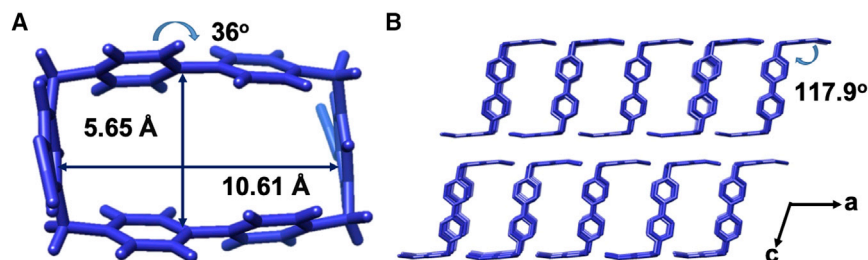


**Figure 2. Solid-state (super)structures of  $m\text{-N}_3\text{-CBPQT}^{4+}$  deduced from single-crystal X-ray diffraction**

(A) Tubular representation showing the distances and the torsional angle associated with the box-like geometry of  $m\text{-N}_3\text{-CBPQT}^{4+}$ .

(B) Tubular representation viewed along the b axis, showing the angle subtended between the azide group and the plane of the box.

mentioning that 2D polymers, synthesized using copper-catalyzed azide-alkyne cycloaddition reactions,<sup>45–47</sup> are amorphous for the most part. Significant challenges remain in using this chemistry to produce highly crystalline materials. To this end, we<sup>48</sup> prepared (Figure 1C) a bisazide-functionalized, rigid, tetracationic cyclophane-based monomer,  $m\text{-N}_3\text{-CBPQT}^{4+}$ . Next, we polymerized this cyclophane with 1,3,5-triethynylbenzene nodes under interfacial copper-catalyzed azide-alkyne cycloaddition conditions. The 2DCBP prepared in this manner has been shown to be composed of crystalline, porous sheets by applying it to a combination of synchrotron X-ray diffraction (XRD), transmission electron microscopy (TEM), electron diffraction, and nitrogen porosimetry. The structural stability of these 2DCBPs has inspired us to deploy them as the active layers in nanofiltration membranes. We have discovered that these membranes exhibit excellent rejection performance in the case of a dye, brilliant blue G, with 99% of it being removed after each cycle. We anticipate that this demonstration will inspire the broad exploration of interfacial click reactions to produce 2DPs and that the potential of host-like building blocks to construct stable macromolecular sheets can act as nanofiltration membranes.

## RESULTS AND DISCUSSION

### Synthesis and characterizations of $m\text{-N}_3\text{-CBPQT}^{4+}$ monomer

The bisazide-functionalized cyclophane monomer,  $m\text{-N}_3\text{-CBPQT}^{4+}$  (1), was synthesized (Figure S1) in four steps following a procedure (see supplemental information) already reported by us<sup>48</sup> in the literature. The monomer was characterized by <sup>1</sup>H nuclear magnetic resonance (NMR) spectroscopy (Figure S3) and single-crystal X-ray crystallography (Figure S5). The single crystals were obtained by slow vapor diffusion of  $i\text{Pr}_2\text{O}$  into a solution of  $m\text{-N}_3\text{-CBPQT}^{4+}$  in MeCN. The box-like cavity of  $m\text{-N}_3\text{-CBPQT}^{4+}$ —measuring 10.61 Å in length and 5.65 Å in width at its periphery and center, respectively (Figure 2A)—is able to host small organic guests. The azide groups are oriented (Figure 2B) out of the box plane, subtending an angle of 118°. Here, we note that  $m\text{-N}_3\text{-CBPQT}^{4+}$  is rigid overall but locally flexible enough to adopt a planar arrangement needed for lateral growth of the polymer during the polymerization. Molecular dynamics simulation of a model trimer constructed from a 1,3,5-triethynylbenzene node and three  $m\text{-N}_3\text{-CBPQT}^{4+}$  units also confirms (Figure S6) the fact that a planar geometry can be achieved starting from the box-like monomer.

### Synthesis of 2DCBP at a liquid-liquid interface

2DCBP was synthesized (Figure 3) from the chloride salt of the  $m\text{-N}_3\text{-CBPQT}^{4+}$  monomer and the commercially available 1,3,5-triethynylbenzene (TEB) node using interfacial

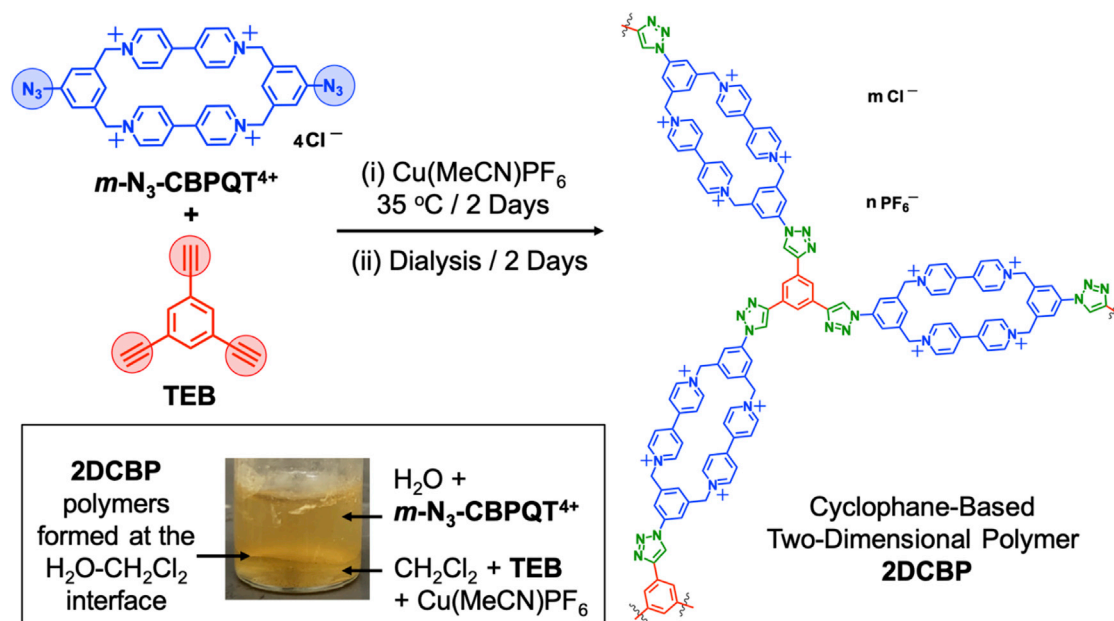


**Figure 3. Schematic representation of the synthesis of 2DCBP**

Left: structural formulas of the monomer and node with polymerizable groups colored in blue and red. Right: structural formula of the repeating unit in the 2DCBP polymer. Inset: photograph of 2DCBP formed at the  $\text{H}_2\text{O}-\text{CH}_2\text{Cl}_2$  interface.

click chemistry (see [supplemental information](#) for a detailed synthetic procedure). In a typical experiment, an aqueous solution of  $m\text{-N}_3\text{-CBPQT}\cdot 4\text{Cl}$  was transferred carefully atop a  $\text{CH}_2\text{Cl}_2$  solution of TEB containing the  $\text{Cu}(\text{MeCN})\text{PF}_6$  catalyst with minimal disturbance of the interfacial layer. The reaction temperature was maintained at  $35^\circ\text{C}$ . The initial pale yellowish color of the solution gradually changed to yellowish brown, and after 2 days robust, dark-brown polymer fragments were observed to be forming only at the  $\text{H}_2\text{O}-\text{CH}_2\text{Cl}_2$  interface. In the course of time, however, larger polymer pieces were observed floating in the aqueous layer. Notably, the formation of 2DCBP was not observed in the absence of the (1) copper catalyst, (2) cyclophane monomer, or (3) TEB node. Collectively, these observations indicate that a copper(I)-mediated azide-alkyne cycloaddition produces triazole units connecting the  $m\text{-N}_3\text{-CBPQT}^{4+}$  monomers with the TEB nodes, yielding 2DCBP. Unreacted monomers, oligomers, and the catalysts were removed ([Figure S2](#)) by dialysis during 2 days against MeOH,  $\text{H}_2\text{O}$ , and MeOH in a sequential manner so as to obtain isolated 2DCBPs dispersed in MeOH. Polymerization in bulk produced random polymeric aggregates ([Figure S14](#)), stressing the importance of interfacial click reaction.

### Characterizations of 2DCBP

Attenuated total reflection infrared spectroscopy confirmed ([Figure 4A](#)) that the expected azide-alkyne click chemistry had occurred at the  $\text{H}_2\text{O}-\text{CH}_2\text{Cl}_2$  interface by the disappearance of the alkyne  $\text{-C}\equiv\text{C-H}$  stretch ( $3,278\text{ cm}^{-1}$ ) on the nodes and the azide  $\text{-N=N=N}$  asymmetric stretch ( $2,117\text{ cm}^{-1}$ ) from the monomers, with a concomitant increase in the stretching frequency at  $3,075\text{ cm}^{-1}$ , which can be associated with the newly formed triazole units in 2DCBP. The solid-state  $^{13}\text{C}$  NMR spectrum of 2DCBP showed signals at approximately 150 and 64 ppm corresponding to triazole units and  $\text{CH}_2$  carbon, respectively. The signal at 143 ppm could be assigned to the  $\text{sp}^2$  quaternary carbons next to the pyridinium nitrogen, and aromatic carbon signals between 120 and 140 ppm to the remaining  $\text{sp}^2$  quaternary carbons ([Figure S4](#)). The UV-visible (UV-vis) absorption spectrum of the 2DCBPs, dispersed in

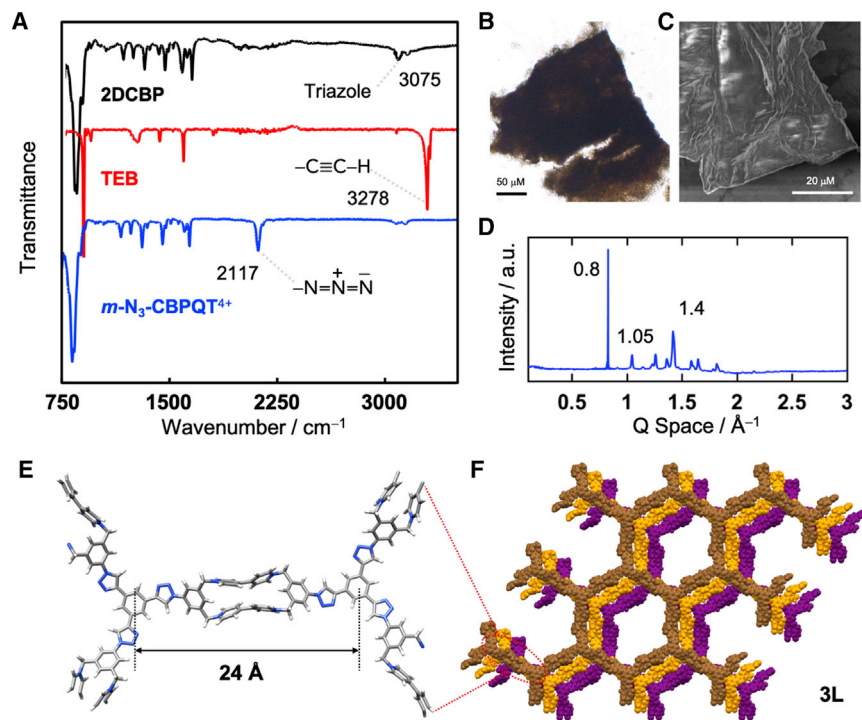


**Figure 4. Characterizations of 2DCBP**

(A) Attenuated total reflection infrared spectroscopy of 2DCBP, TEB, and  $m\text{-N}_3\text{-CBPQT}^{4+}$ . Disappearance of the azide ( $\text{-N=N=N}$ ) asymmetric stretching at  $2,117\text{ cm}^{-1}$  and alkyne ( $\text{-C}\equiv\text{C-H}$ ) stretching at  $3,278\text{ cm}^{-1}$ , and the appearance of triazole stretching frequency ( $3,075\text{ cm}^{-1}$ ) confirmed the fact that the expected azide-alkyne click chemistry had occurred at the  $\text{H}_2\text{O-CH}_2\text{Cl}_2$  interface.

(B and C) (B) Optical micrograph showing a few  $100\text{-}\mu\text{m}$  large dark-brown 2DCBP pieces, and (C) scanning electron micrograph of 2DCBP with sharp edges and wrinkles/folds on the surface.

(D) Synchrotron X-ray diffraction revealing sharp scattering features at  $0.8$ ,  $1.05$ , and  $1.4\text{ \AA}^{-1}$ .

(E and F) (E) Tubular representation displaying a distance of  $\sim 24\text{ \AA}$  between two trisubstituted aromatic rings of DFT-simulated hexagonal 2DCBP structure and (F) plane-view of a space-filling representation of 2DCBP (3L), obtained by DFT calculations, containing three layers.

$\text{H}_2\text{O}$ , displayed (Figure S8) broad absorptions with a red shift of the absorption onset compared with the monomer. The isolated 2DCBPs exhibited (Figure S12) no significant weight loss up to  $\sim 350\text{ }^\circ\text{C}$  and maintained 80% of their initial weight above  $500\text{ }^\circ\text{C}$  under a  $\text{N}_2$  atmosphere. The monomer,  $m\text{-N}_3\text{-CBPQT}^{4+}$ , on the other hand, displayed significant weight loss above  $200\text{ }^\circ\text{C}$  and recorded a  $\sim 60\%$  weight loss around  $300\text{ }^\circ\text{C}$ . All of these pieces of experimental evidence confirm that TEB and  $m\text{-N}_3\text{-CBPQT}^{4+}$  are consumed during the course of the interfacial polymerization, leading to a densely crosslinked network.

The optical (Figure 4B) and scanning electron (Figure 4C) micrographs of as-synthesized 2DCBP revealed the formation of a few hundred micrometer-sized fragments with sharp edges, suggesting that 2DCBP may be crystalline in nature. The scanning electron micrograph displays wrinkles and folds on the surface of the polymer, which are not uncommon features of layered polymeric materials. Synchrotron XRD on 2DCBP exhibited (Figure 4D) sharp scattering features at  $0.8$ ,  $1.05$ , and  $1.4\text{ \AA}^{-1}$ . The sharp in-plane synchrotron diffraction features confirm the fact that the densely crosslinked 2DCBP is structurally regular and highly crystalline. Owing to the presence of (1) a variety of counterions ( $\text{Cl}^-$  from the monomer and  $\text{PF}_6^-$  from the

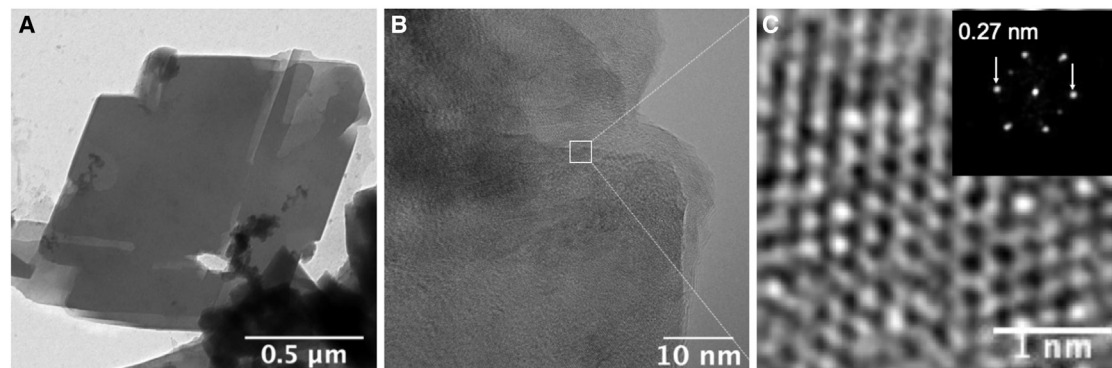


**Figure 5. Transmission electron microscopy of 2DCBP**

(A) Bright-field TEM image displaying layered structure with prominent edges. Different layers of 2DCBP can be visualized from the different contrast of the layers.

(B) High-resolution TEM (HRTEM) image displaying highly isolated faceted sheets with lattice fringes extending throughout the entire polymer particle.

(C) Zoomed-in HRTEM image with the fast Fourier transform pattern at the top right.

catalyst) within the polymer, (2) different interlayer arrangements, (3) the bonding asymmetry of the triazole units, and (4) the local flexibility of the monomer subunits, it is, however, challenging to match a simulated structure or index the Bragg features. Nevertheless, we were able to obtain (Figure S7) the monolayer structure of 2DCBP and its different packing modes (Figure S7) through comprehensive density functional theory (DFT) calculations. For example, the most intense Q peak at  $0.8 \text{ \AA}^{-1}$  can be obtained (Figure 4F) from three layers of packing (3L) of the hexagonal structure of 2DCBP with each adjacent layer displaced by  $8 \text{ \AA}$ .

To develop a deeper understanding of the 2D structure of the polymer, we performed TEM (Figure 5), which reveals (Figure 5A) that the interfacially polymerized 2DCBP is isolated primarily as faceted sheets with lattice fringes extending throughout the entire particle (Figures 5B, S16, and S17). 2D Fourier transform TEM micrographs indicate (Figures 5C, S16B, and S17C) that these polymeric particles feature a hexagonal crystalline lattice, an observation consistent with the synchrotron XRD results and DFT calculations. The dimensions of this lattice are smaller than expected, indicating that these multilayer particles may have noneclipsed interlayer arrangements. The differences between the synchrotron X-ray and TEM results are presumably the result of fundamental factors—while TEM provides the local packing arrangements, XRD considers all types of packing arrangements present in 2DCBP. Further complexity in packing arrangements may also arise on account of generation of defects during irreversible click reactions and sample preparation. Regardless, periodic voids, which are observed in the structure, are consistent with  $\text{N}_2$  sorption experiments that show (Figure S11) conventional type II isotherms with a well-defined pore size of  $1.45 \text{ nm}$ . The Brunauer-Emmett-Teller surface area of 2DCBP was found to be  $76 \text{ m}^2 \text{ g}^{-1}$  while the surface area of the polymer is relatively low, an observation that can presumably be attributed (Figure S18) to the additional mass and occupancy by counterions in the 2DP pores in addition to the offset stacking of the 2DP sheets. Taken together, the various pieces of evidence suggest that the interfacially polymerized 2DCBP fragments are obtained as crystalline, layered particles.

Considering their electroactive tetracationic viologen-based molecular structures, we decided to carry out electrochemistry on both the monomer and the polymer deposited on fluorine-doped tin oxide electrodes by a drop-casting approach. *m*- $\text{N}_3$ -CBPQT $^{4+}$  features (Figure S13) a two-electron reduction peak at  $-0.7 \text{ V}$  versus  $\text{Ag}/\text{AgCl}$ . The first redox wave for the two-electron reduction of viologen units is

not clearly visible in the monomer, suggesting restricted accessibility to the redox-active unit. In contrast, the cyclic voltammogram of 2DCBP exhibited redox waves at both  $-0.05$  and  $-0.5$  V. The observation of the first reduction peak and combined shift of  $-0.2$  V for the second peak in the case of the polymer can be attributed to the additional porosity of the polymer, which assists the diffusion of the electrolyte ions within the channels in the quest to maintain overall electroneutrality.

Sonicated 2DCBP samples remain dispersed (Figure S9) for months in different solvents, such as MeOH, H<sub>2</sub>O, and MeCN, without precipitation, presumably as a result of the positively charged stacked macromolecular sheets—confirmed (Figure S10) by the high average zeta potential value ( $\zeta = 68 \pm 11$  mV)—of 2DCBP particles constructed from the tetracationic cyclophane building blocks. The magnitude of the zeta potential indicates the degree of electrostatic repulsion between adjacent, similarly charged particles in a dispersion. A high zeta potential, therefore, confers stability, i.e., the solution or dispersion will resist aggregation. One might anticipate a charge-repulsion-induced exfoliation of 2DCBP into individual macromolecular sheets, similar to protonation-mediated exfoliation<sup>49</sup> that occurs in covalent organic frameworks (COFs). The presence of counterions within 2DCBP, however, negates the charge repulsion between the individual layers, i.e., the counterions hold these layers firmly together, yielding robust macromolecular assemblies.

### Membrane applications

The well-defined pore size of 2DCBP led us to test its ability to act as a molecular-sieving membrane for water-treatment applications. In this proof-of-concept experiment, the polymer was placed on a polytetrafluoroethylene (PTFE) supporting membrane and used (Figure 6A) to reject the zwitterionic organic Brilliant Blue dye<sup>50</sup> from aqueous solutions in a flow-through mode (Figure 6B). Blank experiments with two  $0.2 \mu\text{m}$  PTFE membranes were run with and without *m*-N<sub>3</sub>-CBPQT<sup>4+</sup> monomers present. Rejection performance was assessed by the optical absorption of 590 nm light using a Varian Cary 5000 Scan Spectrometer. 2DCBP was observed (Figure 6C) to reduce dye concentrations from an initial concentration of  $50 \text{ mg L}^{-1}$  to nondetectable levels in five consecutive cycles. The molecular dimensions of brilliant blue dye molecules are  $1.07 \times 1.47 \times 1.88$  nm, i.e., larger than the pores within the polymer network, which are 1.45 nm in diameter. Hence, dye rejection is attributable to size exclusion as the primary mechanism. We observed that monomer species, deposited as a film, were readily dissolved during the experiment, resulting in no decrease in Brilliant Blue G concentration. Likewise, PTFE filters alone resulted (Figure 6C) in no significant reduction in dye concentrations.

On the other hand, a smaller dye, *syn*-(Me,Me)bimane,<sup>51</sup> with dimensions of  $0.8 \times 0.5 \times 0.2$  nm, passed (Figure S19A) readily through the pores of 2DCBP during similar filtration experiments, an observation consistent with a size-exclusion filtration mechanism. To understand the contributions from sorption and size exclusion,<sup>52</sup> we carried out (Figure S19B) filtration experiments with a large water-soluble cationic dye, protonated 5,10,15,20-tetrakis(4-aminophenyl)porphyrin (TAPP). The fact that 2DCBP recorded an excellent rejection efficiency for this cationic dye strengthens the involvement of a size-exclusion mechanism rather than sorption. Collectively, these findings suggest that the covalently linked, cyclophane-containing 2DPs are required for good membrane performance.

In summary, we have demonstrated interfacial polymerization utilizing azide-alkyne click chemistry to obtain crystalline 2DCBP based on functionalized cyclophane building blocks. These as-synthesized polymer particles are positively charged

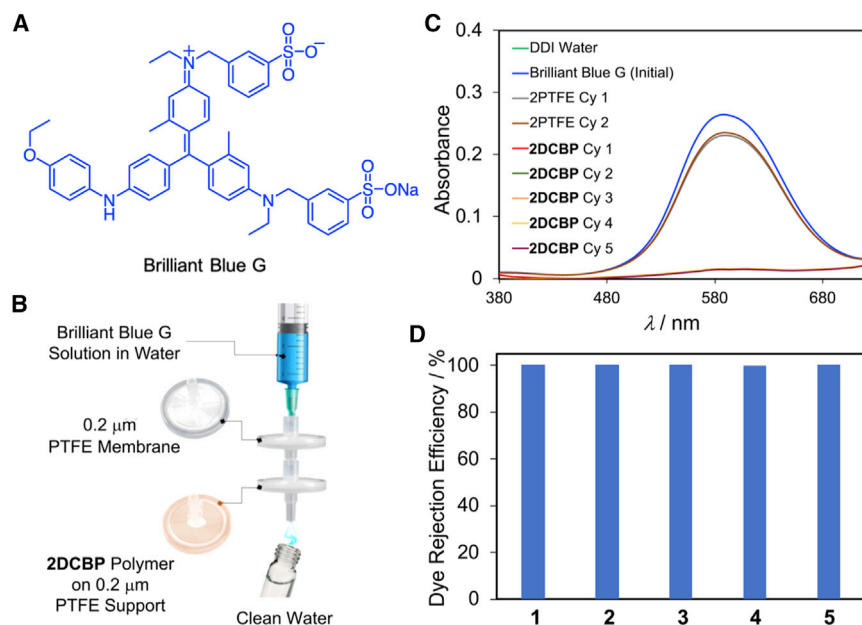


**Figure 6. Membrane application of 2DCBP**  
(A) Structural formula of Brilliant Blue G dye.  
(B) Schematic representation of experimental setup for dye removal or water purification in a flow-through mode. When an aqueous solution of the dye is passed through 2DCBP inserted between two 0.45- $\mu\text{m}$  PTFE membrane filters, clean water is isolated.  
(C) UV-vis spectra of distilled deionized (DDI) water, initial dye solution, dye solution passed through the 2DCBP polymer inserted between two 0.45  $\mu\text{m}$  PTFE membrane filters (2DCBP Cy 1 to 2DCBP Cy 5), and dye solutions passed through two 0.45  $\mu\text{m}$  PTFE membrane filters (control experiments/2PTFE Cy 1 and 2) without 2DCBP.  
(D) Dye-rejection efficiency (%) of 2DCBP polymer in five consecutive cycles. Initial dye concentration = 50 ppm. Solution volume for each cycle = 5 mL. Polymer mass = 5 mg.

and remain dispersed for months in  $\text{H}_2\text{O}$  and  $\text{MeOH}$ . The particles possess multilayered faceted sheet-like morphologies, as revealed by TEM analyses. The structural regularity of these sheets was confirmed by both TEM and synchrotron XRD experiments. The presence of different counterions, diverse interlayer arrangements, and bonding asymmetry of triazole units formed during the irreversible click polymerization process posed challenges in characterizing the complete network. Thorough DFT studies confirmed a layered hexagonal structure of 2DCBP that corroborates both synchrotron diffraction and TEM results. The porous nature of 2DCBP with a well-defined pore size of 1.45 nm, which was measured by nitrogen porosimetry, led us to test it in a proof-of-principle water-purification experiment. The polymer displays an excellent dye rejection capability with dye concentration dropping from an initial concentration of  $50 \text{ mg L}^{-1}$  to nondetectable levels in five consecutive cycles.

In our view, the idea of using host building blocks to construct 2D polymers with a wide range of desirable attributes using a robust synthetic strategy that takes advantage of interfacial click chemistry should be appealing to the 2D polymer and/or COF community. These 2DPs, composed of host molecules, combine their molecular recognition properties and well-defined cavities with the chemical stability, structural regularity, and permanent porosity inherent in the crystalline macromolecular sheets. This confluence of properties can become useful in applications such as chemical and biomolecule sensing, organic electronics, and nanofiltration

membranes. We anticipate that different functionalized host molecules will soon be used as building units for making new 2DPs. By taking advantage of host-guest chemistry, guest molecules can then be used for doping these 2DPs with molecular precision through inclusion complex formation. Appropriate choice of hosts and guest dopants may open up access to 2D polymers for membrane technology and electronic applications.

## EXPERIMENTAL PROCEDURES

Full experimental procedures are provided in the [supplemental experimental procedures](#).

### Resource availability

#### Lead contact

Further information and requests for resources and reagents should be directed to and will be fulfilled by the lead contact, J. Fraser Stoddart ([stoddart@northwestern.edu](mailto:stoddart@northwestern.edu)).

#### Materials availability

All unique and stable reagents generated in this study are available from the lead contact with a completed Materials Transfer Agreement.

#### Data and code availability

This study did not generate and analyze large-scale datasets and custom code. The single-crystal XRD data of  $m\text{-N}_3\text{-CBPQT}\cdot 4\text{PF}_6$  has been deposited in the Cambridge Crystallographic Data Center (CCDC) under accession number CCDC: 2108915. The xyz coordinates and PDB file are freely available under the CC BY 4.0 license on FigShare from the <https://doi.org/10.6084/m9.figshare.16727674>.

### Synthesis of 2DCBP

2DCBP particles were synthesized from the chloride salt of the  $m\text{-N}_3\text{-CBPQT}^{4+}$  monomer and the commercially available 1,3,5-triethynylbenzene (TEB) node using interfacial click chemistry. The  $m\text{-N}_3\text{-CBPQT}\cdot 4\text{Cl}$  monomer (11.2 mg, 0.015 mmol) was dissolved in  $\text{H}_2\text{O}$  (5 mL), providing stock solution A (3 mM). TEB (1.5 mg, 0.01 mmol) and 5 mol %  $\text{Cu}(\text{MeCN})\text{PF}_6$  catalyst were dissolved in  $\text{CH}_2\text{Cl}_2$  (2 mL), providing stock solution B (5 mM). A few drops of dimethylformamide were added to stock B to increase the solubility of TEB. Stock A was transferred carefully atop stock B with minimal disturbance of the interfacial layer. The reaction temperature was maintained at  $35^\circ\text{C}$ . The initial pale yellowish color of the solution gradually changed to yellowish brown, and after 2 days robust, dark-brown polymer fragments were observed to be forming only at the  $\text{H}_2\text{O}\text{-CH}_2\text{Cl}_2$  interface. The reaction mixture was transferred in a Thermo Scientific SnakeSkin tubing (molecular weight cutoff: 3500), and dialysis was performed for 2 days against MeOH,  $\text{H}_2\text{O}$ , and MeOH in a sequential manner to remove unreacted monomers, oligomers, and catalyst. Finally, a 2DCBP dispersion in MeOH was obtained in  $\sim 80\%$  yield and used for further characterization. The interfacial polymerization strategy is scalable. For example, 2DCBP can be synthesized from 112 mg of  $m\text{-N}_3\text{-CBPQT}\cdot 4\text{Cl}$  monomer and 15 mg of TEB irrespective of interfacial area.

### Crystallographic characterization

Single crystals of  $m\text{-N}_3\text{-CBPQT}\cdot 4\text{PF}_6$  were grown by slow vapor diffusion of  $^i\text{Pr}_2\text{O}$  into a solution of  $m\text{-N}_3\text{-CBPQT}^{4+}$  ( $3\text{ mg mL}^{-1}$ ) in MeCN over the course of 4 days. A suitable crystal was selected, and the crystal was mounted on a MITIGEN holder in Paratone oil on a Bruker Kappa APEX CCD area detector diffractometer. The

crystal was kept at 100 K during data collection. Using Olex2, the structure was solved with the ShelXT structure solution program using direct methods and refined with the ShelXL refinement package using least squares minimization.

### Synchrotron powder X-ray diffraction

Synchrotron powder XRD was collected at the Sector 5 DuPont-Northwestern-Dow Collaborative Access Team (DND-CAT) of the Advanced Photon Source (APS), Argonne National Laboratory. Experiments were collected at 17 keV. Exposure times and number of frames were optimized to yield a pattern with low background signal in a reasonable experimental time. All frames were then summed and radially integrated to produce a linear powder XRD pattern using proprietary software available at the APS. All experiments were conducted using a transmission geometry with dried samples placed in 2.0-mm outer diameter borosilicate capillaries with 0.2-mm wall thicknesses purchased from Hilgenberg. The sample-to-detector distance was adjusted to extend across relevant detection ranges of  $q$ . Scattering intensity is reported as a function of the modulus of the scattering vector  $Q$ , related to the scattering angle  $2\theta$  by the equation  $Q = (4\pi/\lambda) \sin\theta$ , where  $\lambda$  is the X-ray wavelength (Equation 1):

$$Q = \frac{4\pi}{\lambda} \sin(\theta). \quad (\text{Equation 1})$$

Scanning electron micrograph images were taken using a Hitachi S-4800 instrument. Samples were prepared by drop-casting 2DCBP on a Si wafer and imaging it without coating.

### Transmission electron microscopy

TEM samples were prepared by drop-casting  $\sim 5 \mu\text{L}$  of the MeOH dispersion of 2DCBP using a micropipette onto lacey-carbon substrate (Cu mesh) TEM grids (Electron Microscopy Sciences, Hatfield, PA). The droplets of the 2DCBP sample were allowed to sit on the grids under ambient conditions for 1 min and were then dried with filter paper. TEM measurements were performed using JEOL ARM 300F and JEOL 2100F instruments operating at 200 keV. Scanning TEM-energy dispersive X-ray spectroscopy data were collected using a Hitachi HD2300 scanning transmission electron microscope.

### Nitrogen porosimetry

Nitrogen isotherm measurements were performed on a Micromeritics Tristar II 3020 (Micromeritics, Norcross, GA) instrument at 77 K with 30–50 mg of sample. Before isotherm measurements were performed, the material was activated by supercritical  $\text{CO}_2$  activation at 40°C. The material was soaked in EtOH overnight and then transferred to a Tousimis Samdri PVT3D critical point drier, in which liquid  $\text{CO}_2$  was used to exchange EtOH four times over 8 h. The material was then heated to 40°C ( $p = 73 \text{ atm}$ ), the critical point of  $\text{CO}_2$ , before the instrument was evacuated at a rate of 0.1 sccm over a period of 12 h.

### DFT analysis

The  $Q$  spacings in the X-ray powder diffraction spectrum were used to deduce the atomistic structures of the 2DCBP. Only the most intense  $Q$  spacing of  $0.8 \text{ \AA}^{-1}$  (8 Å) and the nearest signal at  $1.05 \text{ \AA}^{-1}$  (6 Å) were selected. The distance between the trisubstituted aromatic rings that connect the ends of the triazole-cyclophane-triazole bridges is  $\sim 24 \text{ \AA}$ . The number of layers for these two  $Q$  spacings, therefore, can be deduced from the simple relation  $24 \text{ \AA}/8 \text{ \AA} = 3 \text{ layers}$  (3L), and  $24 \text{ \AA}/6 \text{ \AA} = 4 \text{ layers}$  (4L), respectively. A repeating unit of the 1-layer 2DCBP (1L) was constructed (264 atoms) and optimized with DFT using the Perdew-Burke-Ernzerhof (PBE) functional and double zeta with polarization basis in the Spanish Initiative for Electronic Simulations with Thousands of Atoms (SIESTA, version 4p1-b4) program, using a  $k$  grid of  $3 \times 3 \times 1$ , a density matrix tolerance of

$1.0 \times 10^{-5}$ , a force tolerance of  $0.05 \text{ eV \AA}^{-1}$ , and molecular mechanics potentials that simulate Grimme's dispersion interactions. The two models, 3L and 4L, were generated by vertical displacement of one layer on top of the last and laterally displacing each one in turn by either the  $8 \text{ \AA}$  or  $6 \text{ \AA}$  distance. This procedure was repeated until the 3L and 4L models were built. Because of the bow-shaped curvature in the trisubstituted aromatic nodes, the vertical displacement of  $10 \text{ \AA}$  per layer was chosen, which ensured a suitable interfacial distance of  $3.5 \text{ \AA}$  between the layers with van der Waals radii taken into consideration. The 3L model has 792 atoms and the 4L model has 1,056 atoms. As each repeat unit has 12 cations, 36 positive charges were added to the 3L and 48 to the 4L models, which were optimized with the PBE functional and a single zeta with polarization basis in the SIESTA program using a k grid of  $3 \times 3 \times 1$ , a density matrix tolerance of  $1.0 \times 10^{-4}$ , and a force tolerance of  $0.1 \text{ eV \AA}^{-1}$ .

### SUPPLEMENTAL INFORMATION

Supplemental information can be found online at <https://doi.org/10.1016/j.xcrp.2022.100806>

### ACKNOWLEDGMENTS

The authors would like to thank Northwestern University for their continued support of this research. A.M.E. (DGE-1324585) is supported by the National Science Foundation Graduate Research Fellowship. J.T.H. acknowledges support from the US Department of Energy (DOE), Office of Science, Basic Energy Sciences via grant DE-FG02-08ER15967. L.O.J. and G.C.S. were supported by the Center for the Sustainable Separation of Metals funded by the National Science Foundation (grant no. CHE1925708). Portions of this work were performed at the DND-CAT located at Sector 5 and Sector 8 of the APS. This research used resources of the Advanced Photon Source (APS) and Center for Nanoscale Materials, both US DOE Office of Science User Facilities operated for the DOE Office of Science by Argonne National Laboratory under contract DE-AC02-06CH11357, and the National Energy Research Scientific Computing Center, a DOE Office of Science User Facility supported by the Office of Science of the US DOE under contract no. DE-AC02-05CH11231. Resources at the APS were funded by the National Science Foundation under award 0960140.

### AUTHOR CONTRIBUTIONS

I.R. and J.F.S. conceived the project. I.R., A.M.E., M.A., and J.F.S. prepared the manuscript. I.R. synthesized and characterized the compounds. A.M.E. performed the synchrotron X-ray crystallographic experiments. Y.B. performed single-crystal XRD experiments. I.R. and D.S. performed TEM experiments. S.G. carried out nitrogen sorption and electrochemical experiments. M.R.R. and L.O.J. performed computational studies. I.R. and M.A. performed dye-rejection experiments. All other co-authors contributed to various stages of manuscript preparation.

### DECLARATION OF INTERESTS

The authors declare no competing interests.

Received: September 20, 2021

Revised: December 20, 2021

Accepted: February 17, 2022

Published: March 10, 2022

## REFERENCES

1. Odell, B., Reddington, M.V., Slawin, A.M.Z., Spencer, N., Stoddart, J.F., and Williams, D.J. (1988). Cyclobis(paraquat-*p*-phenylene). A tetracationic multipurpose receptor. *Angew. Chem. Int. Ed.* 27, 1547–1550. <https://doi.org/10.1002/anie.198815471>.
2. Liu, Z., Nalluri, S.K.M., and Stoddart, J.F. (2017). Surveying macrocyclic chemistry: From flexible crown ethers to rigid cyclophanes. *Chem. Soc. Rev.* 46, 2459–2478. <https://doi.org/10.1039/C7CS00185A>.
3. Diederich, F., and Dick, K. (1984). A new water-soluble macrocyclic host of the cyclophane type: host-guest complexation with aromatic guests in aqueous solution and acceleration of the transport of arenes through an aqueous phase. *J. Am. Chem. Soc.* 106, 8024–8036. <https://doi.org/10.1021/ja00338a005>.
4. Cram, D.J., and Cram, J.M. (1997). Container Molecules and Their Guests (Royal Society of Chemistry). <https://doi.org/10.1039/9781847550620>.
5. Liu, W., and Stoddart, J.F. (2021). Emergent behavior in nanoconfined molecular containers. *Chem* 7, 919–947. <https://doi.org/10.1016/j.chempr.2021.02.016>.
6. Bruns, C.J., and Stoddart, J.F. (2016). The Nature of the Mechanical Bond: From Molecules to Machines (John Wiley & Sons, Inc.). <https://doi.org/10.1002/9781119044123>.
7. Yunyan, Q., Yuanning, F., Qing-Hui, G., Astumian, R.D., and Stoddart, J.F. (2020). Pumps through the ages. *Chem* 6, 1952–1977. <https://doi.org/10.1016/j.chempr.2020.07.009>.
8. Barnes, J.C., Juriček, M., Strutt, N.L., Frascioni, M., Sampath, S., Giesener, M.A., et al. (2013). ExBox: A polycyclic aromatic hydrocarbon scavenger. *J. Am. Chem. Soc.* 135, 183–192. <https://doi.org/10.1021/ja307360n>.
9. Shirinfar, B., Ahmed, N., Park, Y.S., Cho, G.-S., Youn, I.S., Han, J.-K., Nam, H.G., and Kim, K.S. (2013). Selective fluorescent detection of RNA in living cells by using imidazolium-based cyclophane. *J. Am. Chem. Soc.* 135, 90–93. <https://doi.org/10.1021/ja3112274>.
10. Zhou, J., Wu, Y., Roy, I., Samanta, A., Stoddart, J.F., Young, R.M., et al. (2019). Choosing sides: Unusual ultrafast charge transfer pathways in an asymmetric electron-accepting cyclophane that binds an electron donor. *Chem. Sci.* 10, 4282–4292. <https://doi.org/10.1039/C8SC05514A>.
11. Juriček, M., Strutt, N.L., Barnes, J.C., Butterfield, A.M., Dale, E.J., Baldrige, K.K., Stoddart, J.F., and Siegel, J.S. (2014). Induced-fit catalysis of corannulene bowl-to-bowl inversion. *Nat. Chem.* 6, 222–228. <https://doi.org/10.1038/nchem.1842>.
12. Coskun, A., Spruell, J.M., Barin, G., Dichtel, W.R., Flood, A.H., Botros, Y.Y., et al. (2012). High hopes: Can molecular electronics realise its potential? *Chem. Soc. Rev.* 41, 4827–4859. <https://doi.org/10.1039/C2CS35053J>.
13. Roy, I., Bobbala, S., Zhou, J., Nguyen, M.T., Nalluri, S.K.M., Wu, Y., et al. (2018). ExTzBox: A glowing cyclophane for live-cell imaging. *J. Am. Chem. Soc.* 140, 7206–7212. <https://doi.org/10.1021/jacs.8b03066>.
14. Roy, I., Bobbala, S., Young, R.M., Beldjoudi, Y., Nguyen, M.T., Cetin, M.M., Cooper, J.A., Allen, S., Anamimoghdam, O., Scott, E.A., et al. (2019). A supramolecular approach for modulated photoprotection, lysosomal delivery, and photodynamic activity of a photosensitizer. *J. Am. Chem. Soc.* 141, 12296–12304. <https://doi.org/10.1021/jacs.9b03990>.
15. Baek, K., Hwang, I., Roy, I., Shetty, D., and Kim, K. (2015). Self-assembly of nanostructured materials through irreversible covalent bond formation. *Acc. Chem. Res.* 48, 2221–2229. <https://doi.org/10.1021/acs.accounts.5b00067>.
16. Baek, K., Yun, G., Kim, Y., Kim, D., Hota, R., Hwang, I., Xu, D., Ko, Y.H., Gu, G.H., Suh, J.H., et al. (2013). Free-standing, single-monomer-thick two-dimensional polymers through covalent self-assembly in solution. *J. Am. Chem. Soc.* 135, 6523–6528. <https://doi.org/10.1021/ja4002019>.
17. Evans, A.M., Ryder, M.R., Flanders, N.C., Vitaku, E., Chen, L.X., and Dichtel, W.R. (2019). Buckling of two-dimensional covalent organic frameworks under thermal stress. *Ind. Eng. Chem. Res.* 58, 9883–9887. <https://doi.org/10.1021/acs.iecr.9b01288>.
18. Jhulki, S., Kim, J., Hwang, I.-C., Haider, G., Park, J., Park, J.Y., Lee, Y., Hwang, W., Dar, A.A., Dhara, B., et al. (2020). Solution-processable, crystalline  $\pi$ -conjugated two-dimensional polymers with high charge carrier mobility. *Chem* 6, 2035–2045. <https://doi.org/10.1016/j.chempr.2020.05.026>.
19. Payamyar, P., King, B.T., O, H.C., Schlu, A.D., and King, B.T. (2016). Two-dimensional polymers: Concepts and perspectives. *Chem. Commun.* 52, 18–34. <https://doi.org/10.1039/c5cc07381b>.
20. Jhulki, S., Evans, A.M., Hao, X.-I., Cooper, M.W., Feriante, C.H., Leisen, J., Li, H., Lam, D., Hersam, M.C., Barlow, S., et al. (2020). Humidity sensing through reversible isomerization of a covalent organic framework. *J. Am. Chem. Soc.* 142, 783–791. <https://doi.org/10.1021/jacs.9b08628>.
21. Meng, Z., Stolz, R.M., and Mirica, K.A. (2019). Two-dimensional chemiresistive covalent organic framework with high intrinsic conductivity. *J. Am. Chem. Soc.* 141, 11929–11937. <https://doi.org/10.1021/jacs.9b03441>.
22. Wu, X., Han, X., Xu, Q., Liu, Y., Yuan, C., Yang, S., Liu, Y., Jiang, J., and Cui, Y. (2019). Chiral BINOL-based covalent organic frameworks for enantioselective sensing. *J. Am. Chem. Soc.* 141, 7081–7089. <https://doi.org/10.1021/jacs.9b02153>.
23. Qian, H.-I., Dai, C., Yang, C.-X., and Yan, X.-P. (2017). High-crystallinity covalent organic framework with dual fluorescence emissions and its ratiometric sensing application. *ACS Appl. Mater. Interfaces* 9, 24999–25005. <https://doi.org/10.1021/acsami.7b08060>.
24. Corcos, A.R., Levato, G.A., Jiang, Z., Evans, A.M., Livingston, A.G., Marin, B.J., and Dichtel, W.R. (2019). Reducing the pore size of covalent organic frameworks in thin-film composite membranes enhances solute rejection. *ACS Mater. Lett.* 1, 440–446. <https://doi.org/10.1021/acsmaterialslett.9b00272>.
25. Wang, S.Z., and Xu, Z.-K. (2019). Ultrathin metal/covalent-organic framework membranes towards ultimate separation. *Chem. Soc. Rev.* 48, 3811–3841. <https://doi.org/10.1039/c9cs00322c>.
26. Fan, H., Gu, J., Meng, H., Knebel, A., and Caro, J. (2018). High-flux membranes based on the covalent organic framework COF-LZU1 for selective dye separation by nanofiltration. *Angew. Chem. Int. Ed.* 57, 4083–4087. <https://doi.org/10.1002/anie.201712816>.
27. Shinde, D.B., Sheng, G., Li, X., Ostwal, M., Emwas, A.-h., Huang, K.-W., et al. (2018). Crystalline 2D covalent organic framework membranes for high-flux organic solvent nanofiltration. *J. Am. Chem. Soc.* 140, 14342–14349. <https://doi.org/10.1021/jacs.8b08788>.
28. Calik, M., Auras, F., Salonen, L.M., Bader, K., Grill, I., Handloser, M., Medina, D.D., Dogru, M., Lo, F., Trauner, D., et al. (2014). Extraction of photogenerated electrons and holes from a covalent organic framework integrated heterojunction. *J. Am. Chem. Soc.* 136, 17802–17807. <https://doi.org/10.1021/ja509551m>.
29. Cai, S.-L., Zhang, Y.-B., Pun, A.B., He, B., Yang, J., Toma, F.M., Sharp, I.D., Yaghi, O.M., Fan, J., Zheng, S.-R., et al. (2014). Tunable electrical conductivity in oriented thin films of tetraiafulvalene-based covalent organic framework. *Chem. Sci.* 5, 4693–4700. <https://doi.org/10.1039/c4sc02593h>.
30. Jin, E., Asada, M., Xu, Q., Dalapati, S., Addicoat, M.A., Brady, M.A., et al. (2017). Two-dimensional  $sp^2$  carbon-conjugated covalent organic frameworks. *Science* 357, 673–676. <https://doi.org/10.1126/science.aan0202>.
31. Geng, K., He, T., Liu, R., Dalapati, S., Tan, K.T., Li, Z., et al. (2020). Covalent organic frameworks: Design, synthesis, and functions. *Chem. Rev.* 120, 8814–8933. <https://doi.org/10.1021/acs.chemrev.9b00550>.
32. Bredas, J.-I., and States, U. (2020). Nucleation–elongation dynamics of two-dimensional covalent organic frameworks. *J. Am. Chem. Soc.* 142, 1367–1374. <https://doi.org/10.1021/jacs.9b10869>.
33. Evans, A.M., Parent, L.R., Flanders, N.C., Bisbey, R.P., Vitaku, E., Kirschner, M.S., Schaller, R.D., Chen, L.X., Gianneschi, N.C., and Dichtel, W.R. (2018). Seeded growth of single-crystal two-dimensional covalent organic frameworks. *Science* 361, 52–57. <https://doi.org/10.1126/science.aar7883>.
34. Lohse, M.S., and Bein, T. (2018). Covalent organic frameworks: Structures, synthesis, and applications. *Adv. Funct. Mater.* 28, 1705553. <https://doi.org/10.1002/adfm.201705553>.
35. Segura, J.L., Mancheño, M.J., and Zamora, F. (2016). Covalent organic frameworks based on Schiff-base chemistry: synthesis, properties and potential applications. *Chem. Soc. Rev.* 45, 5635–5671. <https://doi.org/10.1039/C5CS00878F>.

36. Liu, H., Zhang, Z., Wu, C., Pan, Q., Zhao, Y., and Li, Z. (2019). Interfacial synthesis of conjugated crystalline 2D fluorescent polymer film containing aggregation-induced emission unit. *Small* 15, 1804519. <https://doi.org/10.1002/smll.201804519>.
37. Li, C., Wang, Y., Zou, Y., Zhang, X., Dong, H., and Hu, W. (2020). Two-dimensional conjugated polymer synthesized by interfacial Suzuki reaction: Towards electronic device applications communications *Angew. Chem. Int. Ed.* 59, 9403–9407. <https://doi.org/10.1002/anie.202002644>.
38. Jiang, K., Baburin, I.A., Han, P., Yang, C., Fu, X., Yao, Y., Li, J., Cánovas, E., Seifert, G., Chen, J., and Bonn, M. (2020). Interfacial approach toward benzene-bridged polypyrrole film-based micro-supercapacitors with ultrahigh volumetric power density. *Adv. Funct. Mater.* 30, 1908243. <https://doi.org/10.1002/adfm.201908243>.
39. Zhong, Y., Cheng, B., Park, C., Ray, A., Brown, S., Mujid, F., Kang, K., Sibener, S.J., Muller, D.A., and Park, J. (2019). Wafer-scale synthesis of monolayer two-dimensional porphyrin polymers for hybrid superlattices. *Science* 366, 1379–1384. <https://doi.org/10.1126/science.aax9385>.
40. Zhou, D., Tan, X., Wu, H., Tian, L., and Li, M. (2019). Synthesis of C–C bonded two-dimensional conjugated covalent organic framework films by Suzuki polymerization on a liquid–liquid interface. *Angew. Chem. Int. Ed.* 58, 1376–1381. <https://doi.org/10.1002/anie.201811399>.
41. Ye, X.-L., Huang, Y.-Q., Tang, X.-Y., Xu, J., Peng, C., and Tan, Y.-Z. (2019). Two-dimensional extended  $\pi$ -conjugated triphenylene-core covalent organic polymer. *J. Mater. Chem. A* 7, 3066–3071. <https://doi.org/10.1039/c8ta10554e>.
42. Ratsch, M., Ye, C., Yang, Y., Zhang, A., Evans, A.M., and Bo, K. (2020). All-carbon-linked continuous three-dimensional porous aromatic framework films with nanometer-precise controllable thickness. *J. Am. Chem. Soc.* 142, 6548–6553. <https://doi.org/10.1021/jacs.9b10884>.
43. Huang, D., Qin, A., and Tang, B.Z. (2018). Overview of click polymerization. In *Click Polymerization* (The Royal Society of Chemistry), pp. 1–35.
44. Shi, Y., Cao, X., and Gao, H. (2016). The use of azide-alkyne click chemistry in recent syntheses and applications of polytriazole-based nanostructured polymers. *Nanoscale* 8, 4864–4881. <https://doi.org/10.1039/C5NR09122E>.
45. Gao, T., Su, X., Xu, H., Hu, H., Zeng, C., and Gao, Y. (2020). Construction of the copper-functionalized covalent organic framework used as a heterogeneous catalyst for click reaction. *ChemistrySelect* 5, 15010–15014. <https://doi.org/10.1002/slct.202004130>.
46. Komeda, J., Shiotsuki, R., Rapakousiou, A., Sakamoto, R., Toyoda, R., Iwase, K., Tsuji, M., Kamiya, K., and Nishihara, H. (2020). ‘Click’ conjugated porous polymer nanofilm with a large domain size created by a liquid/liquid interfacial protocol. *Chem. Commun.* 56, 3677–3680. <https://doi.org/10.1039/D0CC00360C>.
47. Lindemann, P., Schade, A., Monnereau, L., Feng, W., Batra, K., Gliemann, H., Levkin, P., Bräse, S., Wöll, C., and Tsotsalas, M. (2016). Surface functionalization of conjugated microporous polymer thin films and nanomembranes using orthogonal chemistries. *J. Mater. Chem. A* 4, 6815–6818. <https://doi.org/10.1039/C5TA09429A>.
48. Burke, D.W., Sun, C., Castano, I., Flanders, N.C., Evans, A.M., Vitaku, E., McLeod, D.C., Lambeth, R.H., Chen, L.X., Gianneschi, N.C., and Dichtel, W.R. (2020). Acid exfoliation of imine-linked covalent organic frameworks enables solution processing into crystalline thin films. *Angew. Chem. Int. Ed.* 27, 5165–5171. <https://doi.org/10.1002/anie.201913975>.
49. Wu, Z., Joo, H., Ahn, I.-S., Kim, J.-H., Kim, C.-K., and Lee, K. (2004). Design of doped hybrid xerogels for a controlled release of brilliant blue FCF. *J. Non-cryst. Sol.* 342, 46–53. <https://doi.org/10.1016/j.jnoncrsol.2004.06.004>.
50. Roy, A., Das, P.J., Diskin-Posner, Y., Firer, M., Grynszpan, F., and Montag, M. (2018). Quenching of syn-bimane fluorescence by Na<sup>+</sup> complexation. *New J. Chem.* 42, 15541–15545. <https://doi.org/10.1039/C8NJ01945B>.
51. Fenton, J.L., Burke, D.W., Qian, D., Olvera de la Cruz, M., and Dichtel, W.R. (2021). Polycrystalline covalent organic framework films act as adsorbents, not membranes. *J. Am. Chem. Soc.* 143, 1466–1473. <https://doi.org/10.1021/jacs.0c11159>.
52. Lipke, M.C., Wu, Y., Roy, I., Wang, Y., Wasielewski, M.R., and Stoddart, J.F. (2018). Shuttling rates, electronic states, and hysteresis in a ring-in-ring rotaxane. *ACS Cent. Sci.* 4, 362–371. <https://doi.org/10.1021/acscentsci.7b00535>.